Mouse and computational models link Mlc2v dephosphorylation to altered myosin kinetics in early cardiac disease

Farah Sheikh,[1] Kunfu Ouyang,[1] Stuart G. Campbell,[2] Robert C. Lyon,[1] Joyce Chuang,[1,2] Dan Fitzsimons,[3] Jared Tangney,[2] Carlos G. Hidalgo,[4] Charles S. Chung,[4] Hongqiang Cheng,[1] Nancy D. Dalton,[1] Yusu Gu,[1] Hideko Kasahara,[5] Majid Ghassemian,[6,7] Jeffrey H. Omens,[1,2] Kirk L. Peterson,[1] Henk L. Granzier,[4] Richard L. Moss,[3] Andrew D. McCulloch,[2] and Ju Chen[1]

[1]Department of Medicine and [2]Department of Bioengineering, UCSD, La Jolla, California, USA. [3]Department of Cell and Regenerative Biology, University of Wisconsin School of Medicine and Public Health, Madison, Wisconsin, USA. [4]Departments of Physiology and Molecular and Cellular Biology, University of Arizona, Tucson, Arizona, USA. [5]Department of Physiology and Functional Genomics, University of Florida College of Medicine, Gainesville, Florida, USA. [6]Department of Chemistry and [7]Department of Biochemistry, UCSD, La Jolla, California, USA.

Actin-myosin interactions provide the driving force underlying each heartbeat. The current view is that actin-bound regulatory proteins play a dominant role in the activation of calcium-dependent cardiac muscle contraction. In contrast, the relevance and nature of regulation by myosin regulatory proteins (for example, myosin light chain-2 [MLC2]) in cardiac muscle remain poorly understood. By integrating gene-targeted mouse and computational models, we have identified an indispensable role for ventricular Mlc2 (Mlc2v) phosphorylation in regulating cardiac muscle contraction. Cardiac myosin cycling kinetics, which directly control actin-myosin interactions, were directly affected, but surprisingly, Mlc2v phosphorylation also fed back to cooperatively influence calcium-dependent activation of the thin filament. Loss of these mechanisms produced early defects in the rate of cardiac muscle twitch relaxation and ventricular torsion. Strikingly, these defects preceded the left ventricular dysfunction of heart disease and failure in a mouse model with nonphosphorylatable Mlc2v. Thus, there is a direct and early role for Mlc2 phosphorylation in regulating actin-myosin interactions in striated muscle contraction, and dephosphorylation of Mlc2 or loss of these mechanisms can play a critical role in heart failure.

Introduction

Interactions between the contractile proteins myosin and actin provide the driving force for muscle contraction (1). However, the molecular mechanisms underlying the regulation of these interactions in striated muscle, such as cardiac muscle, which are fundamental to heart function and are of central importance in heart disease and failure in humans, are still not well understood (2). For the last 5 decades, the simplistic obligatory step of Ca^{2+} binding to actin-bound regulatory proteins (e.g., troponin-tropomyosin complex) has contributed to the prevailing view that the control of calcium cycling and actin-bound regulatory proteins (thin filament proteins) dominates regulation of muscle contraction (3, 4) as well as underlies the dysregulation of contractile dynamics in heart failure. In contrast, myosin regulatory proteins (thick filament proteins), such as the ventricular form of myosin light chain-2 (MLC2v), are viewed to play lesser roles (5), and thus, their regulation and function remain poorly understood in this context and especially in vivo.

Growing evidence suggests that this simple model cannot explain all aspects of striated muscle regulation and that myosin regulatory proteins, such as MLC2v, may have an influential role in regulating activation of cardiac muscle contraction via post-translational modifications such as phosphorylation (6–14). In the 1980s, in vitro studies performed by Stull and colleagues noted a temporal association between the extent of Mlc phosphorylation and potentiation of isometric twitch force in skeletal muscle (5), suggesting that Ca^{2+} binding to actin-bound regulatory proteins (troponin C) may not be the only process regulating striated muscle contraction. Although the precise role and nature of this regulation still remains unknown in striated muscle, information gained from in vitro and structural studies led to the hypothesis that the negative charge from phosphorylation may act to structurally repel the myosin heads away from the thick filament backbone and toward actin (15–17). However, recent studies in isolated skeletal muscle myosins suggest that this mechanism does not explain the observed changes in myosin mechanics and provide some evidence to support a hypothesis that Mlc2 phosphorylation may act to regulate stiffness of the myosin lever arm, which thereby prolongs myosin (crossbridge) duty cycle (18). Previous studies suggest that the myosin neck domain contains an elastic region, which generates strain-dependent forces to generate motion (19). There is also some in vitro evidence suggesting that MLC2 phosphorylation may affect stiffness of the myosin lever arm and/or hinge region in smooth muscle (20).

Ca^{2+} regulation of contraction in striated muscle appears to be a highly cooperative process, as is clearly evident in the steepness of force-pCa relationships when describing Ca^{2+} sensitivity of force, with the greatest cooperativity observed when myosin binds strongly to actin in an intact thin filament (9). We and others have previously reported that positive cooperative mechanisms contribute to several properties of activation of cardiac muscle contraction

Authorship note: Farah Sheikh, Kunfu Ouyang, and Stuart G. Campbell contributed equally to this work.

Conflict of interest: The authors have declared that no conflict of interest exists.

Citation for this article: *J Clin Invest.* 2012;122(4):1209–1221. doi:10.1172/JCI61134.

primarily involving Ca^{2+}-mediated activation via actin-bound regulatory proteins involving the cardiac thin filament (9, 21–23). The question of whether and how myosin regulatory proteins, such as MLC2, influence these cooperative mechanisms and effects in contracting living cardiac muscles remains to be directly addressed. Understanding the molecular actions of MLC2v phosphorylation in the regulation of actin-myosin interaction kinetics in cardiac muscle is of key importance, since emerging evidence in humans suggests a critical role for MLC2v in human health. Several studies have shown that dysregulation of MLC2v via dephosphorylation is associated with human cardiomyopathies and heart failure (6, 8, 10–14); however, mechanistic insights into its underlying role in heart disease still remain elusive.

In the present study, we reveal a direct role for Mlc2v phosphorylation in actin-myosin regulation and cardiac disease in vivo by using an integrative combination of gene-targeted animal and multiscale computational models. We show in living contracting cardiac muscles that Mlc2v phosphorylation dynamically controls myosin cycling kinetics and activation of cardiac muscle contraction via 2 molecular mechanisms, which cooperatively control the overall number of crossbridge attachments (increased myosin head repulsion from thick filament toward actin) and the transition of crossbridge attachments to the strongly bound, force-generating state (increased myosin neck domain stiffness). Loss of these mechanisms uncovers previously unrecognized defects in the rates of twitch relaxation and spatial mechanics involving ventricular torsion, which strikingly precede the functional deficits of heart disease and failure in a nonphosphorylatable Mlc2v mouse model. We propose a new model of actin-myosin regulation, which includes myosin-driven mechanisms whereby Mlc2v Ser14/Ser15 phosphorylation (a) directly influences actin-myosin interactions independently of actin-bound regulatory proteins, which in turn have the ability to (b) cooperatively feedback to influence calcium activation of thin filaments. These mechanisms regulate function of cardiac muscle at multiple levels, including crossbridge cycling kinetics at the level of myosin heavy chain, cardiac muscle Ca^{2+} sensitivity of force at the level of the myofilament, and twitch dynamics in intact cardiac muscle as well as ventricular torsion, pump function, and adverse structural remodeling in disease, leading to heart failure at the organ level.

Results

Loss of Mlc2v Ser14/Ser15 is necessary and sufficient to reduce endogenous Mlc2v phosphorylation in vivo. To determine the functional importance of the regulatory protein Mlc2v via its phosphorylation, we generated 2 Mlc2v phosphorylation mutant mouse lines (Supplemental Figure 1; supplemental material available online with this article; doi:10.1172/JCI61134DS1). Although the regulation of MLC2v phosphorylation in vivo remains unclear, it is thought that Ser15 on Mlc2v is the major phosphorylation site regulating muscle function in rodents and humans (6, 10, 13, 14, 24–26), while Ser14 is also thought to be important for stretch-activation responses in muscle (24). To determine the role or roles of Mlc2v Ser15 and Ser14 phosphorylation sites in vivo, we generated knockin mutant mice changing Ser15 to Ala15 (S15A) as well as Ser14 and Ser15 to Ala14 and Ala15 (S14A/S15A), respectively (Supplemental Figure 1). Incorporation of the mutations in both S15A (single mutant [SM]) and S14A/S15A (double mutant [DM]) mice was confirmed using DNA analyses (Supplemental Figure 1). The endogenous regulation of Mlc2v phosphorylation in our knockin mice was analyzed using 2D gel analysis and mass spectrometry of myofilament proteins (Figure 1, A and B). WT hearts showed approximately 31% Mlc2v phosphorylation (Figure 1A), corresponding to phosphorylation at sites Ser15 and Ser19 (Figure 1B). Surprisingly, SM mutant hearts displayed a compensatory increase in Mlc2v phosphorylation (Figure 1A), which was due to an endogenous switch to Ser14 phosphorylation (Figure 1B). Loss of Mlc2v phosphorylation was seen only in DM mutant myocardium, where there was loss of Ser14 and Ser15 phosphorylation (Figure 1, A and B). These results suggest that the contribution of Ser19, important for smooth muscle Mlc2 phosphorylation (27), is likely negligible in regulating endogenous Mlc2v phosphorylation in DM cardiac muscle. MLC kinase (Mlck) phosphorylation assays (Figure 1, C and D) also revealed a significant decrease in Mlc2v phosphorylation in DM mutant mice. An alignment of mouse striated versus smooth muscle/nonmuscle MLC highlights differences surrounding Ser14/Ser15 and Ser19 phosphorylation sites (Supplemental Figure 2).

Loss of Mlc2v Ser14/Ser15 phosphorylation in vivo predisposes mice to dilated cardiomyopathy, heart failure, and premature death. DM mutant mice are viable at birth; however, they display a striking susceptibility to premature death (Figure 2A, DM vs. WT and SM, $P < 0.01$) as a consequence of dilated cardiomyopathy (DCM), leading to heart failure (Figure 2, B–E). Features of DM mutant hearts included significant increases in (a) ventricular weight to body weight ratios (Figure 2B); (b) age-dependent cardiac chamber enlargement and wall thinning, which was accompanied by a significant decrease in cardiac function (Figure 2, C and D) that is classically associated with DCM leading to heart failure; (c) early changes in cardiomyocyte length (Figure 2E); and (d) classical ultrastructural sarcomeric defects, including significant Z-line thickening at 6 months of age (Figure 2F). The chamber dilation, depressed cardiac function, and premature death observed in DM mutant mice were not evident in SM mice (Figure 2A [WT vs. SM, $P = 0.425$], Figure 2B, Supplemental Figure 3), suggesting that the endogenous switch to Ser14 phosphorylation (Figure 1, A and B) is sufficient to functionally compensate for the loss of MLC2v residue Ser15 in vivo. Most remarkably, the heart muscle defects observed in a majority of DM mutant mice were not associated with significant changes in the cardiac expression of fetal genes, which is classically associated with early signs of cardiac stress (Supplemental Figure 4A). In addition, the majority of DM mutant mice did not exhibit signs of heart muscle damage or fibrosis when compared with WT and SM (Supplemental Figure 4B) mice. However, in sporadic cases, a subset (10%) of DM mutant mice displayed heterogeneous calcification and fibrosis most prominently in the ventricular endocardium associated with low-level expression of a single fetal gene, β-myosin heavy chain (β-MHC) (Supplemental Figure 5), highlighting a more severe consequence of the loss of the Mlc2v phosphorylation gradient upon the subendocardial layer of the heart.

Mlc2v phosphorylation directly controls early cardiac muscle relaxation twitch kinetics. To determine the primary functional defect in cardiac muscle associated with end-stage heart disease and failure in DM mutant mice, we simultaneously measured twitch tension and Ca^{2+} transients in intact papillary muscles isolated from young WT and DM mutant mice at 6 weeks of age. Although DM mutant mice showed no defects in myocardial ultrastructure, dimensions, and global cardiac function at this age when compared with WT mice (Figure 2G and Supplemental Figure 6), measurements in intact muscle did reveal differences in the magnitude and timing

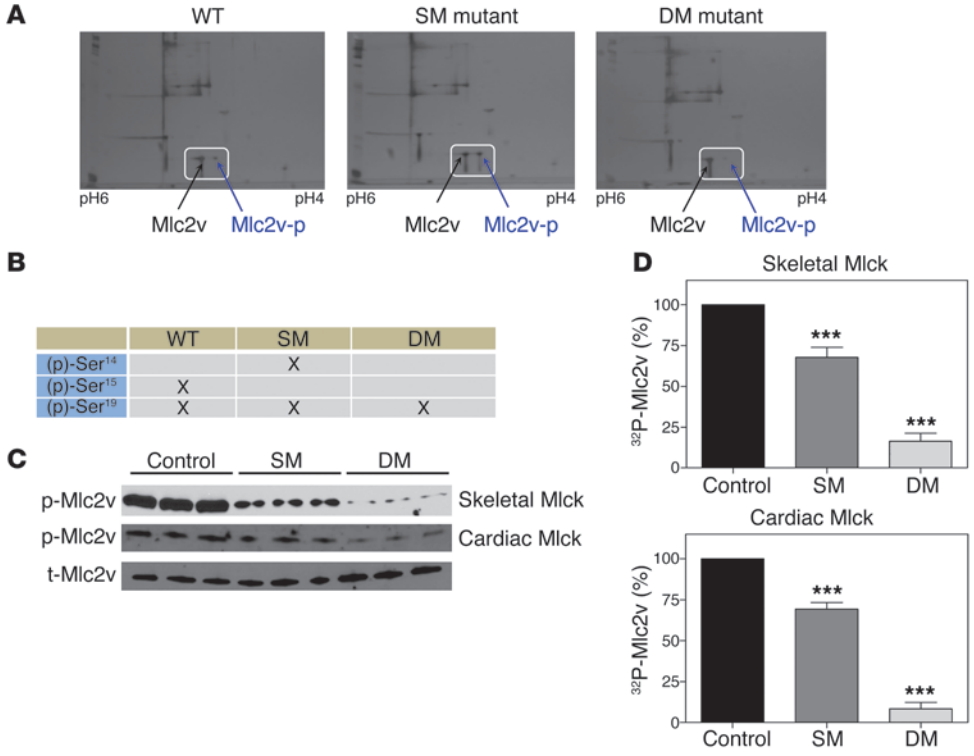

Figure 1

Assessment of endogenous Mlc2v phosphorylation in *Mlc2v* mutant mouse lines in vivo. (**A**) 2D gel analysis of Mlc2v in myofilament proteins in mice at 6 weeks of age. Silver-stained gels were used to determine percentage of Mlc2v phosphorylation (Mlc2v-p) by densitometry as shown in the representative gels. Unphosphorylated (left) and phosphorylated (p) (right) Moc2v are highlighted in gels. (**B**) Summary chart depicting the mass spectrometry analysis of endogenous Mlc2v Ser14, Ser15, and Ser19 phosphorylation in myofilament proteins in mice at 6 weeks of age. (**C**) Representative autoradiograms show levels of phosphorylated Mlc2v (Mlc2v-p) catalyzed by skeletal (top panel) and cardiac (middle panel) Mlck in mice ($n = 3$). Total Mlc2v (t-Mlc2v) is shown as a loading control. (**D**) Phosphorylated Mlc2v protein catalyzed by skeletal (top) and cardiac (bottom) Mlck was quantified through liquid scintillation counting in SM and DM mutant mice and expressed as a percentage of WT, which are set to 100%. Percentage values are expressed as mean ± SEM ($n = 3$). ***$P < 0.001$.

of twitch tension (Figure 2H). The most notable change was a significant acceleration of twitch relaxation in DM mutant versus WT muscles (Figure 2H). These specific twitch contraction defects were observed both at room temperature and 37°C (Figure 2H and Supplemental Figure 7), indicating a robust response that would be present in DM mutant mice under physiological conditions. Moreover, altered twitch dynamics in DM mutant muscles were not the result of altered calcium cycling, since the amplitude and time course of intracellular Ca^{2+} transients were not significantly different between DM mutant and WT muscles (Figure 2H), further suggesting a nonstatic relationship between Ca^{2+} transients and muscle twitch tension. These results suggest what we believe to be a novel role for Mlc2v phosphorylation as a determinant of the kinetics of cardiac muscle relaxation.

A computational model uncovers dual molecular actions of Mlc2v phosphorylation in regulating Ca^{2+} sensitivity and twitch kinetics of cardiac muscle in vitro. To define the precise molecular mechanisms underlying the effects of Mlc2v phosphorylation on muscle contraction, we created a multiscale computational model based on our recent computational model of cooperative myofilament activation (21). This approach allows testing of 2 hypothesized molecular mechanisms for a direct effect of Mlc2v phosphorylation on the kinetics of actin-myosin regulation of striated muscle (Figure 3, A–C). The first postulated mechanism is that the addition of a negatively charged phosphate group on Mlc2v repels myosin heads away from the thick filament backbone to increase myosin head diffusion toward actin (15–17), thereby enhancing the formation of actin-myosin crossbridges (mechanism 1; Figure 3A). The second postulated mechanism is based on recent studies demonstrating that Mlc phosphorylation decreases actin filament sliding velocity, which is consistent with an increase in myosin duty cycle caused by myosin lever arm stiffening (18). These studies, along with studies in smooth muscle, suggest the second mechanism whereby Mlc2 phosphorylation increases the stiffness of the myosin lever arm (18, 20) and alters crossbridge kinetics (mechanism 2; Figure 3B). We used transition state theory and a thermodynamic analysis of the power stroke to derive the forward and reverse rates of the myosin power stroke as a function of lever arm stiffness (Figure 3C, Supplemental Methods, and Supplemental Figure 8). This mechanistic approach was critical in that it allowed the putative effects of phosphorylation to be constrained in the model using just 2 parameters.

Hallmark biophysical effects of increased Mlc2v phosphorylation (via MLC kinase treatment) in skinned myocardium include increases in maximum contraction force (maximum tension) and the Ca^{2+} sensitivity of contraction force (pCa_{50}), with no detectable changes in the kinetics of force redevelopment following stretch (k_{tr}) (28, 29). We exploited the model and these functional observations to determine whether these mechanisms (or both in combination) could quantitatively reproduce all of the observations in skinned cardiac myofilaments (28, 29). Simulations show that neither mechanism 1 nor mechanism 2 alone would be capable of simultaneously matching all the reported hallmark effects of increased Mlc2v phosphorylation in skinned cardiac myofilaments (Figure 3D). However, when approximately equal contributions of both mechanisms are introduced into the model (fit values in Supplemental Tables 1 and 2), the resulting simulations capture all of the published phosphorylation-dependent alterations (refs. 28, 29, and Figure 3D), including the full steady-state force-pCa relation reported in mouse skinned myocardium (Figure 3E). Interestingly, we did not observe significant differences in

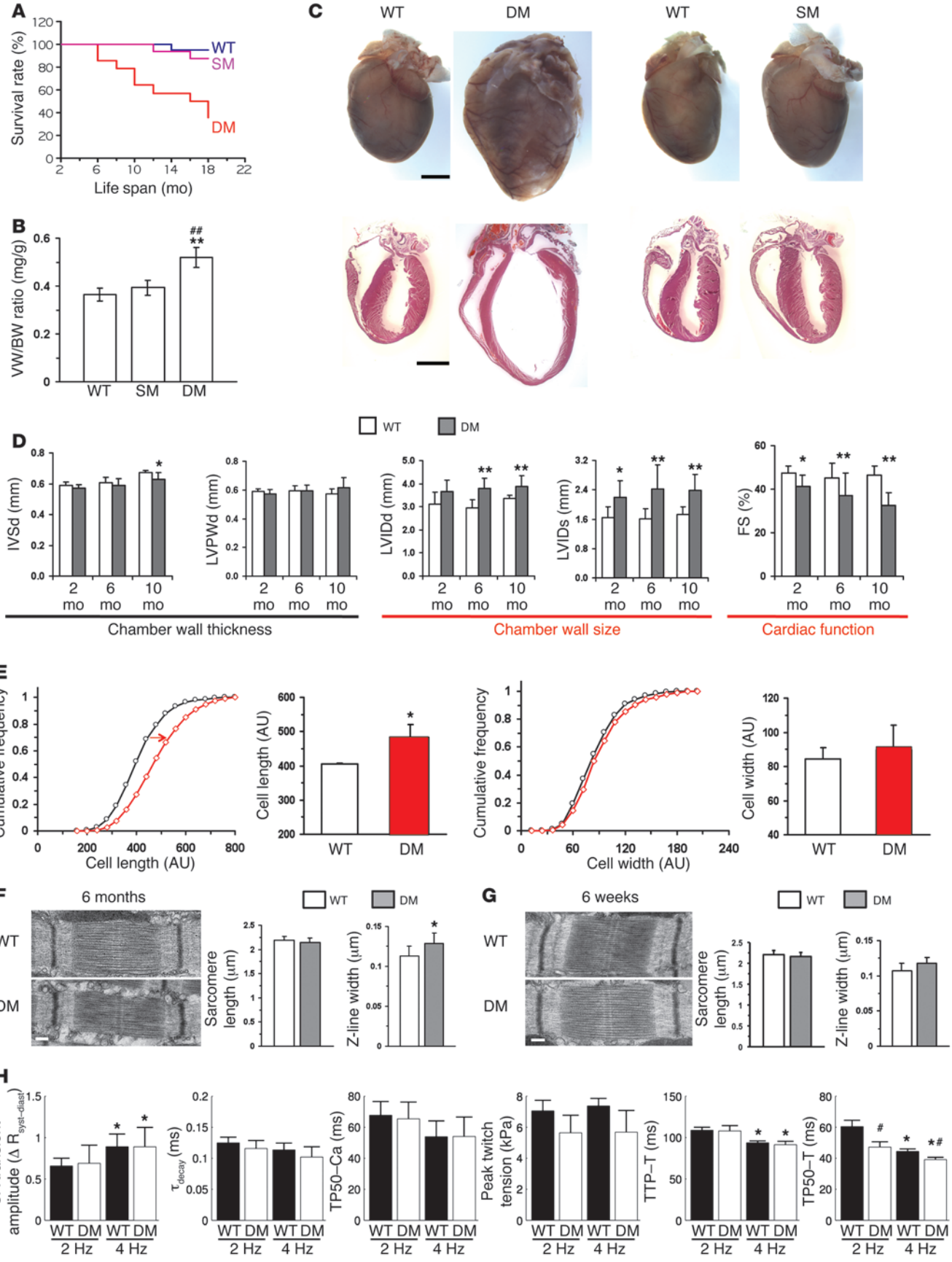
A
Survival rate (%)
120
100
80
60
40
20
0
2
6
10
14
18
22
Life span (mo)
WT
SM
DM
B
VW/BW ratio (mg/g)
0.6
0.4
0.2
0
##
**
WT
SM
DM
C
WT
DM
WT
SM
D
WT
DM
IVSd (mm)
LVPWd (mm)
LVIDd (mm)
LVIDs (mm)
FS (%)
2 mo
6 mo
10 mo
Chamber wall thickness
Chamber wall size
Cardiac function
E
Cumulative frequency
Cell length (AU)
Cell width (AU)
F
6 months
WT
DM
Sarcomere length (μm)
Z-line width (μm)
G
6 weeks
H
CA transient amplitude (Δ R syst–diast)
τdecay (ms)
TP50–Ca (ms)
Peak twitch tension (kPa)
TTP–T (ms)
TP50–T (ms)
WT DM WT DM
2 Hz
4 Hz

Figure 2
DM mice display premature death due to heart failure and early cardiac twitch relaxation defects. (**A**) Kaplan-Meier survival analysis. (**B**) Ventricular weight to body weight ratios (VW/BW) in WT (n = 7), SM (n = 10), and DM (n = 5) mice. $^{**}P < 0.01$ DM versus WT; $^{\#\#}P < 0.01$ DM versus SM. (**C**) Whole mouse heart (top) and H&E-stained sections (bottom). Scale bars: 2 mm. (**D**) Echocardiographic measurements from WT (n = 6, 2 months; n = 10, 6 months; n = 10, 10 months) and DM (n = 6, 2 months; n = 9, 6 months; n = 8, 10 months) mice. IVSd: interventricular septal wall thickness at end diastole; LVPWd: LV posterior wall thickness at end diastole; LVIDd/LVIDs: LV internal dimension at end diastole and at end systole; FS (%), LV fractional shortening. $^{*}P < 0.05$; $^{**}P < 0.01$. (**E**) Cardiomyocyte dimensions in WT (black line, n = 3) and DM (red line, n = 3) mice at 6 months. Arrow shows shift in cell length. $^{*}P < 0.05$. (**F** and **G**) Electron micrographs from mouse LV at (**F**) 6 months and (**G**) 6 weeks. Sarcomere length and Z-line widths (n = >100 per heart, n = 3). Scale bars: 200 nm. $^{*}P < 0.05$. (**H**) WT (n = 9) and DM (n = 7) Ca^{2+} and twitch transients. $\Delta R_{syst-diast}$, change in Fura-2 fluorescence ratio; τ_{decay}, Ca^{2+} transient decay time constant; TP50-Ca (–T), time from peak to 50% (tension transient) decay; TTP-T, time from stimulus to peak tension. $^{*}P < 0.05$ versus same group at 2 Hz; $^{\#}P < 0.05$ versus WT at same pacing frequency. Data are expressed as mean values ± SEM.

the relationship of k_{tr} versus force between WT and DM mutant skinned cardiac myofilaments (data not shown), which is also consistent with published data on the effects of phosphorylation on k_{tr} (28) and further validates the use of this computational model to recapitulate effects of Mlc2v phosphorylation/dephosphorylation in cardiac myofilaments. Results from the model (based on fit values in Supplemental Table 2) could also be used to quantify the "magnitude" of effects of Mlc2v phosphorylation on crossbridge cycling kinetics, which would otherwise be difficult to do solely using biophysical approaches, and included a 2.6-fold increase in the rate of crossbridge attachment and a 23% increase in crossbridge stiffness for phosphorylated myosin when computational simulations fit the experimental data in skinned cardiac myofilaments (29). In order to rule out the possibility that other combinations of attachment and stiffness values could also reproduce the same measured effects of phosphorylation, we performed more than 3,600 additional simulations using pairs of wide-ranging attachment/stiffness values (Supplemental Figure 9). We showed that the 2 fitted attachment/stiffness parameter values in our model uniquely reproduce the 3 hallmark experimentally measured (maximum tension, Ca^{2+} sensitivity, maximum k_{tr}) effects of Mlc2v phosphorylation, highlighting the robustness and predictive value of our model (Supplemental Figure 9). These data and combination of mechanisms suggest that Mlc2v phosphorylation has dual molecular roles in "accelerating" (increased rate of myosin attachment due to electrostatic effect) and "braking" (slowing of the crossbridge power stroke step due to elevated lever arm stiffness) separate aspects of crossbridge cycling kinetics. These events result in an increased accumulation (~1:1 to ~6:1) of crossbridges in the prepower stroke, non–force generating state (M_{pr}; Figure 3C). Crossbridges in this attached state are now in a position to fine-tune myofilament Ca^{2+} sensitivity of force by allowing myosin to be cooperatively recruited to neighboring actin-binding sites to sustain thin filament activation and prolong contraction/relaxation without causing an unrealistic increase in maximum contraction force (Figure 3, C and D). To extend our mechanistic observations and understand the impact of Mlc2v phosphorylation on thin filament regulation, we disabled the structural link between cooperating thin filament regulatory proteins (e.g., tropomyosin interactions) to effectively abolish cooperativity between myosin and these neighboring thin filament regulatory proteins that was inherent to the model while leaving both phosphorylation mechanisms in place (Figure 3D). Under these conditions, the effects of Mlc2v phosphorylation on Ca^{2+} sensitivity of force were blunted (Figure 3D), highlighting the existence of positive cooperative feedback mechanisms (cooperative recruitment) involving myosin. These data suggest that the thin filament structure (e.g., tropomyosin-tropomyosin structural interactions along the thin filaments) is sensitized to small changes in phosphorylation-dependent behavior of cardiac muscle myosin.

We next exploited the computational model to simulate the effects of these mechanisms on isometric twitch tension driven by measured calcium transients and found that the 2 molecular mechanisms in combination were also sufficient to predict the differences in twitch dynamics (magnitude and timing) observed between WT and DM mutant mice with high fidelity in the absence of differences in calcium cycling kinetics (Figure 3F). In particular, time from peak tension to 50% relaxation was 43.2 ms in the predicted twitch, which was essentially identical to the mean value of 43.1 ± 1.3 ms measured in WT papillary muscles (Figure 3G). The accuracy of this prediction provides strong evidence that the molecular mechanisms underlying the effects of Mlc2v phosphorylation (mechanisms 1 and 2) can explain the accelerated twitch relaxation observed in DM mutant muscles.

Mlc2v phosphorylation-dependent mechanisms regulate regional mechanics of the myocardium and LV torsion in vivo. To determine how primary defects in myosin kinetics resulting from loss of Mlc2v phosphorylation could affect the heart in vivo, we first assessed the endogenous spatial Mlc2v phosphorylation pattern in the mouse heart. We show that Mlc2v phosphorylation was heterogeneous and existed as a transmural gradient in the mouse LV wall (Figure 4A), decreasing from epicardium to endocardium (44.4% ± 9.6% vs. 30.2% ± 4.5%; $P < 0.03$), which is consistent with previous reports in rodent and human hearts (6, 30). Since it has been proposed that this gradient may contribute to the twisting motion of the ventricles (torsion) during systole (6), we used finite element models of LV mechanics driven by WT (phosphorylation gradient) or DM mutant (no phosphorylation gradient) twitch characteristics (Figure 4B and Supplemental Tables 2–4) to test the hypothesis that absence of Mlc2v phosphorylation gradients would alter LV regional wall mechanics and torsion. Simulations representing the absence of Mlc2v phosphorylation exhibited strikingly lower values of peak LV torsion (twist) throughout systole, as well as a lower untwisting rate in diastole (Figure 4B). To further test these model predictions in vivo, the time course of LV torsion was measured in young WT and DM mutant mice at 6 weeks of age (Figure 4C) using phase-tagged MRI. The time course of torsion measured in DM mutant hearts was significantly altered from that measured in WT mice ($P < 0.05$). Peak torsion in DM mutant mice at 6 weeks of age was significantly reduced relative to WT (36 ± 5 vs. 49 ± 2 degrees cm^{-1}), and mirrored the difference predicted by the model (37.9 vs. 43.4 degrees cm^{-1}) (Figure 4B). Torsion measurements also showed reduced rates of LV untwisting in diastole that agreed with predictions (Figure 4B). No significant differences in global cardiac function as measured by percentage of ejection fraction (EF) in MRI sequences were observed between WT and DM mutant hearts at this stage (63.4% ± 2.1% vs. 62.4% ± 1.3%,

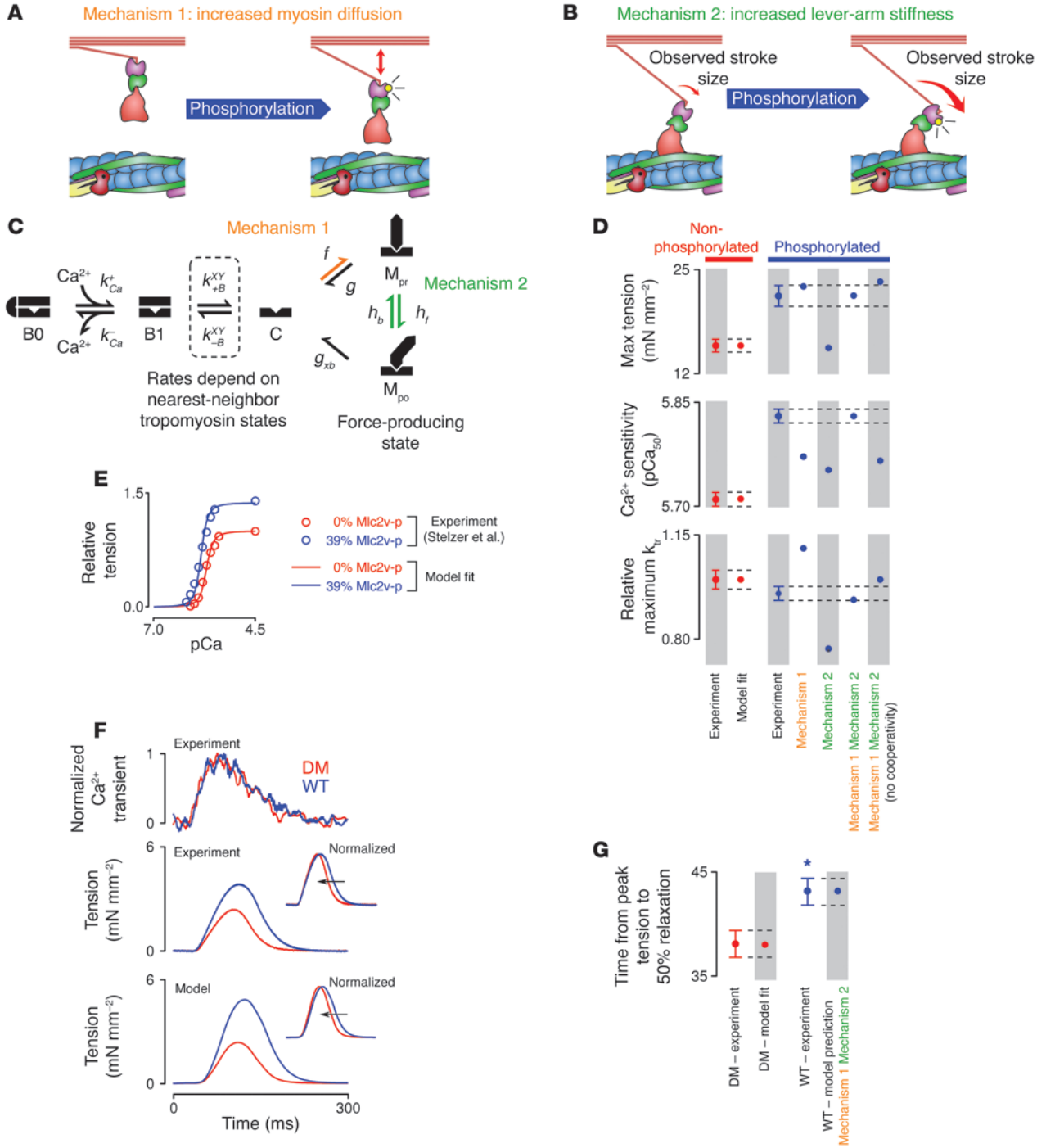

Figure 3

A computational model identifies dual molecular roles for ventricular Mlc2 phosphorylation (Mlc2v-p) in regulating cardiac actin-myosin interactions that underlie twitch relaxation defects in DM mice. The effects of Mlc2v-p on (**A**) myosin head diffusion (17) and (**B**) myosin lever arm stiffness (18, 20) were tested. (**C**) A recent model of myofilament function (21) was modified to include Mlc2v-p mechanisms (orange, mechanism 1; green, mechanism 2). Refer to Supplemental Methods and Supplemental Tables 1 and 2 for details. (**D**) Model parameters for 0% Mlc2v-p were adjusted such that model fit matched maximum tension, Ca^{2+} sensitivity to force (pCa_{50}), and relative maximum rate of force redevelopment (k_{tr}) in dephosphorylated skinned mouse myocardium (28, 29). Model fit to experimental data in phosphorylated skinned myocardium (28, 29) was obtained with both mechanisms. (**E**) Model fits (lines) to experimental data from steady-state force-pCa curves measured in dephosphorylated (red circle) and phosphorylated (blue circle) skinned myocardium (digitized from Stelzer et al., ref. 29) were only obtained with both mechanisms. (**F**) Ca^{2+} transient and muscle twitch tension measurements in 6-week-old papillary muscles at 25°C. Muscle simulations used parameters of 0% (red trace) and 31% MLC2v-p (blue trace, value measured in WT myocardium in Figure 1A). Maximum tension and twitch relaxation defects in DM muscle were recapitulated by model simulations. Arrow denotes leftward shift (acceleration) when normalized to tension. Values for fit are in Supplemental Tables 1 and 2. (**G**) Model fit of TP50-T in WT and DM muscle using both mechanisms is shown.

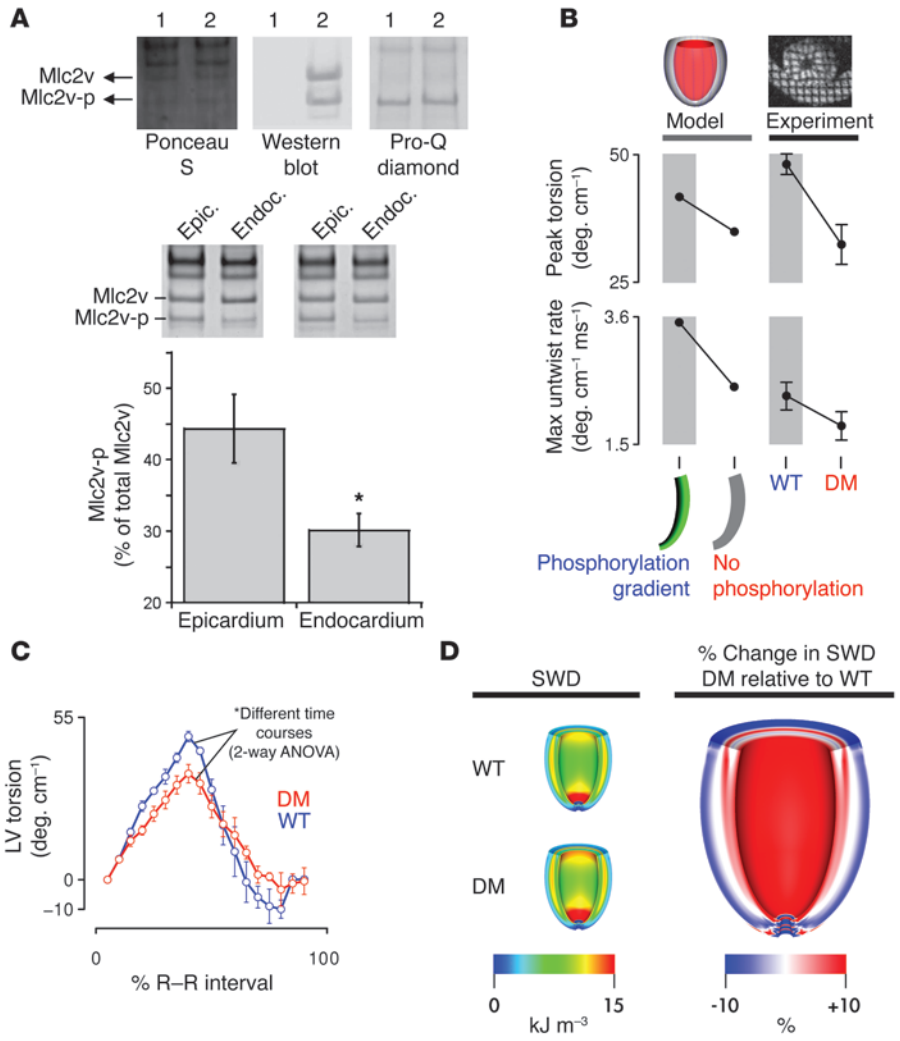

Figure 4
Mlc2v phosphorylation–mediated mechanisms underlie the prefailure defects in ventricular torsion and subendocardial workload in DM mutant hearts in vivo. (**A**) LV proteins were separated by urea-glycerol-PAGE, transferred to PVDF, and stained with Ponceau S (top, left panel) and blotted with no primary antibody control (lane 1) or Mlc2v antibodies (lane 2) (top, middle panel). A separate gel was stained with phospho-specific Pro-Q Diamond stain (top, right panel). Combined methods identified Mlc2v and Mlc2v-p bands. Middle panel: urea-glycerol-PAGE analysis of Mlc2v and Mlc2v-p in LV epicardial and endocardial samples from mice. Bottom panel: integrated optical density method was used to determine Mlc2v-p level in the LV epicardium and endocardium as a percentage of Mlc2v. Data are expressed as mean ± SEM ($n = 4$). *$P < 0.05$. (**B**) Finite element model of LV function was driven by Mlc2v phosphorylation–dependent mechanisms to test the effects of 0% (no phosphorylation gradient) and 15% (phosphorylation gradient) transmural gradients on simulated ventricular torsion over the cardiac cycle, as expressed as peak torsion (systole) and maximum untwist rate (diastole). (**C**) Ventricular torsion analysis in WT (blue trace) and DM (red trace) hearts is shown using tagged MRI. Values are expressed as mean ± SEM ($n = 3$). (**D**) 2D spatial simulations of mechanical work done by muscle fibers across the LV wall during the cardiac cycle (cardiac SWD) in WT and DM mutant hearts. Percentage change in SWD in DM relative to WT hearts is shown. Parameters used in multiscale finite element models are given in Supplemental Tables 1–5.

respectively), suggesting that the early torsion defects were not due to decreased global ventricular ejection. Replacement of the transmural gradient with a uniform Mlc2v phosphorylation having the same mean value throughout the LV wall did not maintain torsion to the extent experimentally observed in WT hearts in vivo (data not shown), further validating the importance of these gradients in normal cardiac function.

Spatial Mlc2v phosphorylation-dependent mechanisms have an impact on myofiber strain kinetics across the heart wall to control cardiac function and disease. To determine how early loss of Mlc2v phosphorylation spatial gradients and underlying defects in torsion might account for DCM and heart failure in DM mutant mice, we exploited the finite element model to test the hypothesis that the distribution of regional myofiber stroke work density (SWD) or workload throughout the myocardium (epicardium to endocardium) may be affected in the DM mutant model (Figure 4D). Model predictions demonstrate that to maintain EF in the absence of Mlc2v phosphorylation, the DM mutant heart would have to undergo an approximately 10% increase in subendocardial myofiber SWD above WT hearts (Figure 4D). This suggests that loss of phosphorylation and the consequent decrease in twist redistributes stress and strain in myofibers across the wall, with adverse consequences for subendocardial workload (Figure 4D). The deleterious consequences of this increased, abnormal subendocardial workload is highlighted by the (a) increased disease vulnerability of the ventricular subendocardium in a subset of DM mutant mice exhibiting DCM (Supplemental Figure 5) and (b) increased vulnerability of young DM mutant mice to DCM following induction of mechanical (LV pressure overload) stress at a stage when no structural/disease alterations are observed (Figure 5). Pressure overload induced different myocardial growth responses in DM mutant compared with WT mice undergoing similar molecular and transstenotic pressure gradient stresses (Figure 5), in the sense that DM mutant hearts exhibited early increases in chamber size only and not chamber wall thickness, indicative of DCM, as opposed to expected increases in both chamber size and wall thickness observed in WT hearts, which typically undergo concentric hypertrophy (Figure 5A). Cardiomyocytes from DM mutant mice exhibited these same early growth response defects following pressure overload in that cell length was increased only in DM mutant mice, while cell width was expectedly increased in WT mice (Figure 5B). This further suggests that defects in myofiber strain kinetics as a consequence of reduced transmural gradients in

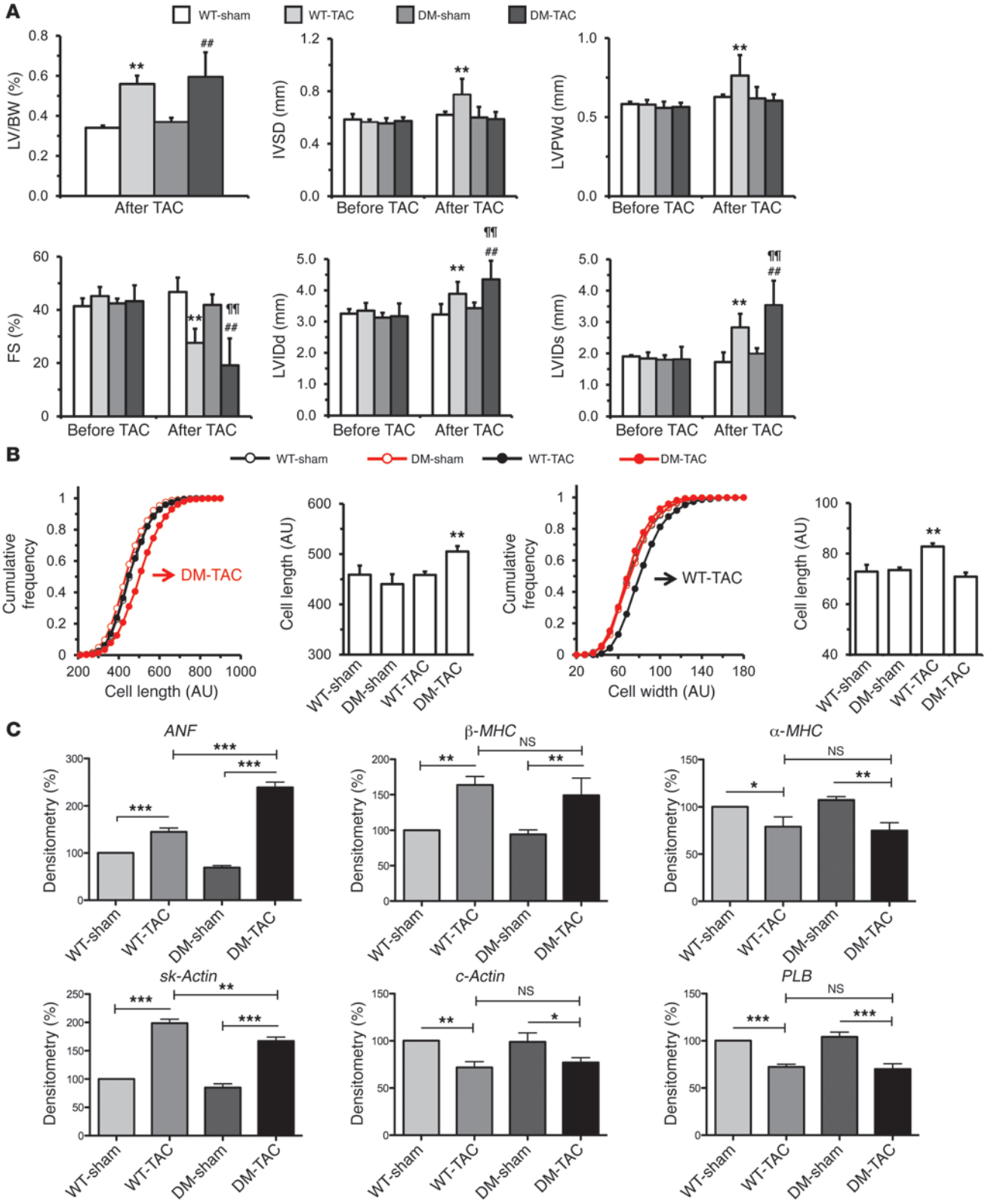
A
WT-sham
WT-TAC
DM-sham
DM-TAC
LV/BW (%)
IVSD (mm)
LVPWd (mm)
FS (%)
LVIDd (mm)
LVIDs (mm)
After TAC
Before TAC
B
Cumulative frequency
DM-TAC
Cell length (AU)
WT-TAC
Cell width (AU)
C
ANF
β-MHC
α-MHC
sk-Actin
c-Actin
PLB
Densitometry (%)
NS

Figure 5
DM mutant mice are sensitized to pressure overload following TAC. (**A**) LV to BW ratios as well as in vivo echocardiographic assessment of cardiac size and function in 6-week-old WT and DM mutant mice, before (pre) and following (post) sham and TAC operation for 1 week. $^{**}P < 0.01$ versus WT-sham; $^{\#\#}P < 0.01$ versus DM-sham, ¶¶$P < 0.01$ versus WT-TAC. Transstenotic pressure gradients within WT (82.35 ± 10.8 mmHg; $n = 7$) and DM (78.05 ± 9.7 mmHg; $n = 7$) hearts were not significantly different. No significant changes in heart rates were observed between mice between groups. (**B**) Cardiomyocyte length and widths are plotted from WT (black line; $n = 3$) versus DM (red line; $n = 3$) mice before and after sham and TAC operation for 1 week. Red arrow highlights shift toward higher cardiomyocyte length in DM-TAC. Data are expressed as AU. Left shift representative of increased cell width was only observed in cardiomyocytes isolated from WT-TAC. $^{**}P < 0.01$ (**C**) *ANF*, β-*MHC*, α-*MHC*, *sk-Actin*, *c-Actin*, and *PLB* RNA expression in LV from mice before and after sham and TAC operation for 1 week ($n = 3$ in each group) are normalized to *Gapdh* RNA expression and expressed as a percentage (%) of WT-sham controls, which are set to 100%. $^{*}P < 0.05$; $^{**}P < 0.01$; $^{***}P < 0.001$. Data are expressed as mean values ± SEM.

Mlc2v phosphorylation and posttranslational modifications at the level of myosin may also be important in the adaptation of the cardiomyocyte to changes in shape/geometry.

Discussion

The precise role of Mlc2 and the mechanisms underlying its direct regulation in muscle have remained under debate since the discovery of Mlc2 in 1969 (31, 32). Electron microscopy and optical diffraction studies have provided indirect evidence in support of a hypothesis that Mlc2 phosphorylation alters the structural disposition of crossbridges through molecular interactions involving charge repulsion and diffusion of the myosin heads away from the thick filament (15–17, 33). Recent in vitro studies using isolated myosins highlight a second hypothesis, that Mlc2 phosphorylation may function to regulate the crossbridge by altering the elasticity of the myosin lever arm by stiffening the lever arm to increase myosin duty cycle (18, 20). Nonetheless, whether Mlcs are directly involved in the regulation of actin-myosin interactions or play a role in disease and by which mechanisms are not yet known. In this study, we utilize integrative gene-targeted mouse and multiscale computational models to bridge the gap between experimental results at the molecular and physiological levels as a means to identify roles and mechanisms for the involvement of Mlc2 in regulating actin-myosin interactions in cardiac muscle and disease in vivo (Figure 6).

The utility of this integrative approach was first highlighted in our studies focused on understanding the mechanisms for a potential role for Mlc2v phosphorylation in crossbridge cycling kinetics by exploiting published biological data from skinned cardiac myofilaments. Specifically, when 2 hypothesized molecular actions of Mlc2v phosphorylation (increased myosin diffusion and myosin lever arm stiffness represented by only 2 parameters) were introduced into the computational model as a means of including phosphorylation-mediated changes in cardiac myosin behavior, both were required to quantitatively recapitulate 3 previously published hallmark experimental effects of Mlc2v phosphorylation in skinned cardiac myofilaments (Figure 3). These data provided evidence for a direct role for Mlc2v phosphorylation in regulating actin-myosin interactions in cardiac muscle while identifying the underlying mechanisms driving phosphorylation-mediated effects on cardiac myosin cycling kinetics. This combination of mechanisms suggested dual counteractive molecular actions of Mlc2v phosphorylation. These included molecular actions of accelerating (increased rate of myosin attachment due to electrostatic effect) and braking (slowing of the crossbridge power stroke step due to elevated lever arm stiffness) separate aspects of crossbridge cycling kinetics, resulting in an accumulation of strongly bound (attached) crossbridges (Figure 3). These attached crossbridges can then fine-tune myofilament Ca^{2+} sensitivity of force, since they allow myosin to be cooperatively recruited to neighboring actin-binding sites to sustain thin filament activation and prolong the contraction/relaxation cycle without causing an unrealistic increase in maximum contraction force. An important extension of this mechanism was highlighted in the model when the structural link between cooperative thin filament regulatory proteins (e.g., tropomyosin interactions) was disabled to abolish cooperation between myosin and these neighboring thin filament regulatory proteins, causing the effects of Mlc2v phosphorylation on Ca^{2+} sensitivity of force to be blunted (Figure 3D). These data suggest the importance of positive feedback mechanisms involving cardiac myosin, which influence calcium-dependent activation of the thin filament in order to fine-tune force development and its regulation by calcium at the level of the cardiac myofilament.

The concept of Mlc2v phosphorylation mediating myosin's role in feedback control is integral to understanding its actions on twitch dynamics in intact cardiac muscle, since the twitch is produced by complex feedback behavior between calcium regulation (Ca^{2+} activation of thin filaments) and crossbridge cycling kinetics (cooperative binding of myosin to thin filaments). We show through integrative approaches that the primary prefailure effect due to loss of Mlc2v phosphorylation in intact DM mutant cardiac muscle is an acceleration of cardiac twitch relaxation, which was also predicted by mechanisms in the computational model (Figure 3, F and G). An important aspect of these observations is that the defects in twitch dynamics in DM mutant mice were observed independently of changes in Ca^{2+} delivery (Figure 2H and Figure 3F), highlighting an adaptable relationship between Ca^{2+} transients and muscle twitch tension as opposed to the static relationship that was previously accepted as accurate. In other words, regardless of rising and declining Ca^{2+} concentrations in muscle, Mlc2v phosphorylation would independently regulate the number of strongly bound crossbridge attachments as well as myosin's ability to cooperatively recruit actin-binding sites to sustain thin filament activation and prolong the contraction/relaxation cycle. The mechanisms underlying the computational model further demonstrate that loss of phosphorylation decreases the number of strongly bound crossbridge attachments, reducing the ability of myosin to cooperatively sustain thin filament activation, leading to an acceleration of twitch relaxation independent of changes to Ca^{2+}, which further explains the mechanisms underlying the twitch defects in DM mutant cardiac muscle. Thus, these integrative approaches reveal (a) unappreciated roles for Mlc2v phosphorylation and myosin for feedback control of calcium-dependent activation of the thin filament (Figure 6B) and (b) the molecular basis for early alterations in myofilament function that precede classic early alterations (ultrastructural, calcium cycling) associated with heart disease and failure in DM mutant mice.

Our integrative approaches further uncover unrecognized prefailure effects of myosin cycling kinetics due to the loss of Mlc2v phosphorylation, which we hypothesized and now show to have

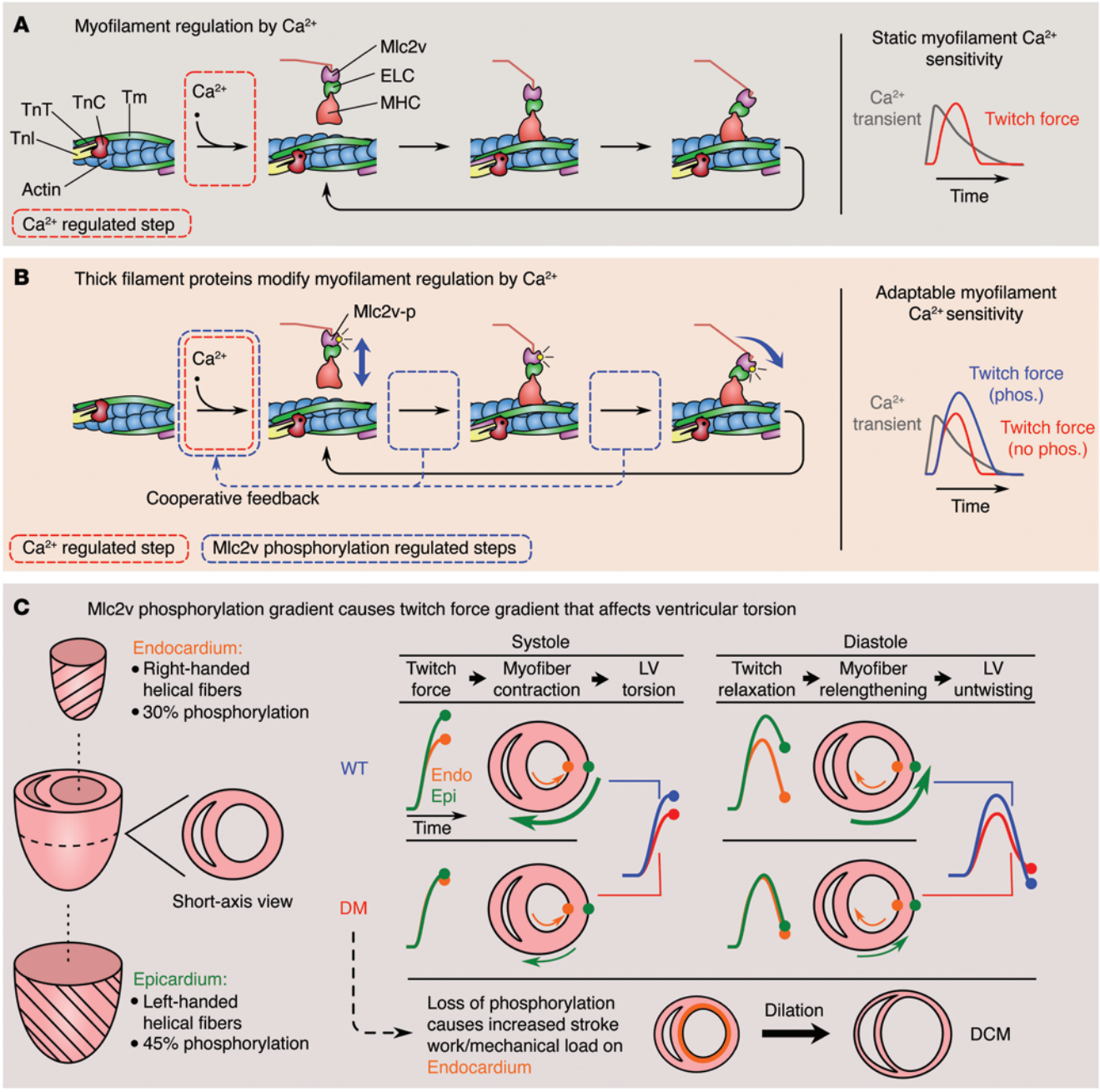

Figure 6

Schematic model linking Mlc2v phosphorylation to twitch dynamics, ventricular mechanics, and early cardiac disease events. (**A**) The traditional view of myofilament regulation is that binding of Ca^{2+} to troponin C (TnC) induces shifting of tropomyosin (Tm) to expose myosin binding sites on the actin filament. This implies a static relationship between the Ca^{2+} transient and twitch tension, with Ca^{2+} signaling as the primary determinant of twitch dynamics. (**B**) Our new evidence shows that posttranslational modification of thick filament proteins (e.g., Mlc2v phosphorylation) alters Ca^{2+} sensitivity of the filaments, highlighting a previously unappreciated adaptable relationship. Mlc2v phosphorylation simultaneously increases myosin binding and myosin lever arm stiffness, altering kinetics of crossbridge cycling (shown by dashed blue boxes) to increase crossbridge duty ratio. This phosphorylation-dependent behavior of myosin can positively cooperative to influence calcium-dependent activation and kinetics of the thin filament by allowing crossbridges to cooperatively activate neighboring binding sites on actin (dashed blue arrow). (**C**) Mlc2v phosphorylation can regulate ventricular torsion because Mlc2v phosphorylation levels vary through the LV wall. Higher phosphorylation in the left-handed helical fibers of WT epicardium enhances their twitch tension and consequently peak torsion compared with DM mice. Because elevated Mlc2v phosphorylation also lengthens twitch duration, diastolic untwisting in WT mice is dominated by epicardial fibers. Without opposition by right-handed endocardial fibers, the untwisting rate is increased relative to DM. Meeting hemodynamic demand without the benefit of epicardial Mlc2v hyperphosphorylation elevates endocardial workload in DM mice, contributing to DCM and heart failure (bottom).

an impact on LV torsion mechanics in hearts in vivo (Figure 4). The basis for the hypothesis comes from our studies, which agree well with the results by Davis et al. (6), which highlight the existence of a transmural Mlc2v phosphorylation gradient in the mouse LV wall, decreasing from epicardium to endocardium (Figure 4A). The mechanisms underlying ventricular torsion are not fully understood; however, 2 postulated contributing factors are the helical orientation of epicardial and endocardial myofiber sheets within the LV wall and the anisotropy of myocardial stress-strain properties (34). Epicardial fibers are oriented in a left-handed helix along the wall, while endocardial fibers follow a right-handed helical path (Figure 6C). Epicardial myofibers are thought to direct torsion during systole (left handed) and untwisting rate during diastole (right handed) because their position is further from the center of rotation, resulting in a longer moment arm and greater movement (34, 35).

It remains unclear whether underlying variations in myosin cycling kinetics imposed by Mlc2v phosphorylation-mediated mechanisms contribute to this differential regulation of epicardial versus endocardial tension development and recovery. We show that the computational model is able to predict similar defects in LV torsion throughout systole and untwisting rate in diastole that were also subsequently observed in prefailure DM mutant hearts in vivo (Figure 4B). The mechanisms in our model suggest that these spatial gradients and variations in myosin cycling kinetics in the LV wall drive torsion/twist mechanics by regulating both the magnitude and duration of twitch force and myocardial contraction (Figure 6C). In WT hearts, endocardial myofibers relax first (due to low phosphorylation, resulting in smaller forces and shorter twitch duration), while the epicardial myofibers contract late and unopposed to endocardial myofibers (due to high phosphorylation, resulting in larger forces and prolonged twitch duration, which delays contraction), thereby driving and enhancing torsion in systole and untwisting rate in diastole. The consequent reduction of Mlc2v phosphorylation gradients in the LV wall (a) reduces the magnitude of forces in the epicardium to now equal magnitude of force in the endocardium (resulting in homogenous distribution across wall) and (b) accelerates twitch relaxation/duration in the epicardium to now directly match the timing of twitch force in the endocardium (causing forces to directly oppose and negate one another), thus reducing the imposed mechanical advantage of the epicardium to drive torsion and untwisting in DM mutant hearts in vivo. These studies highlight the critical importance of myosin cycling kinetics in regulating regional cardiac mechanics linked to LV torsion and their impact on early cardiac remodeling events leading to disease. This may have important translational implications, since torsion is severely depressed in patients with DCM (35, 36) and is emerging as an early clinical predictor of heart disease in children and adults (35, 37–41); however, the mechanism or mechanisms underlying this phenomenon are unknown. Thus, our integrative models can be exploited as tools to investigate mechanisms underlying LV torsion in humans, since torsion is thought to be physiologically equivalent in mice and humans (34). Future testable hypotheses could include expanding our computational models to include the effects of stiffness, stretch-induced tension, fiber orientation, and ion channel function (since repolarization currents vary between epicardium and endocardium) to predict how these variables affect regional muscle mechanics (torsion, workload distribution, function) in the heart.

We also provide evidence that spatial Mlc2v phosphorylation-dependent mechanisms and loss of torsion have a direct impact on myofiber strain kinetics across the heart wall to control cardiac function and disease. The computational model predicted that loss of Mlc2v phosphorylation would render the subendocardial layer of the heart vulnerable to increased workload as a consequence of the loss of torsion (Figure 4D). Consequences of this increased subendocardial workload were evident in DM mutant mice by the (a) presence of subendocardial fibrosis and calcification in a subset (10%) of DM mutant hearts exhibiting DCM (Supplemental Figure 5) and (b) vulnerability of young DM mutant mice to subendocardial dilation and DCM following imposition of mechanical stress at a stage when no cardiac architectural alterations are evident (Figure 5). Since cardiac muscle cell growth defects were also observed in young DM mutant mice following mechanical stress consistent with eccentric as opposed to concentric hypertrophy, this further suggested that Mlc2v Ser14/Ser15 phosphorylation sites and myosin may also act as critical signaling effectors for strains/stress, which can signal early adaptive changes in cardiomyocyte shape that may be important in the compensatory pathological changes (wall thickening) evoked by stress leading to cardiomyopathies, such as DCM. This may also have translational implications, since the subendocardial myofibers are thought to be particularly vulnerable in patients with DCM, but the etiology remains unknown (42). Thus, our studies offer insights and tools (computational and mouse models) to expand our understanding of how variations in myosin cycling kinetics across the heart wall contribute to decreased subendocardial workload and DCM. This is important, since we highlight a direct and early influence of loss of Mlc2v phosphorylation in heart disease and failure in vivo (Figure 2), suggesting a direct contribution of dysregulation of MLC2v phosphorylation in human cardiomyopathy and failure (6, 8, 10–14). Recent studies suggest that the MLCK family of "cytoskeletal protein kinases," which target Mlc2v phosphorylation, might also have a broader role in mechanosignaling (43) and thus future studies focused on determining whether strain modulation of cardiac Mlck activity is a potential contributing factor to the mechanisms and outcomes highlighted by our models are warranted.

Taken together, our data highlight how multiscale computational models can be combined with traditional genetic mouse models and biological findings to identify key aspects of complex and dynamic mechanisms (variations in myosin cycling kinetics as a result of spatial gradients in posttranslational modifications of cardiac proteins) underlying early events in the pathogenesis of diseases, such as DCM, which would not be possible to do solely using traditional approaches. Specifically, our integrative approaches were critical in (a) refining current perceptions of actin-myosin regulatory mechanisms in cardiac muscle while resolving a direct and early influence for Mlc2v in heart failure; (b) revealing a previously unappreciated role for cytoskeletal Mlc2v-based (myosin) phosphorylation gradients in the regulation of LV torsion and normal cardiac function, which may have important translational implications in applying stem cell and tissue engineering approaches as therapies for cardiac muscle dysfunction and disease; and (c) identifying new tools to exploit our understanding of early events (and mechanisms) in heart disease, which have important translational implications in potential medical applications of these findings in terms of improved diagnosis, detection, and management of early events in heart disease (e.g.,

develop more sophisticated multiscale models to uncover early targets of disease and develop sensitive methods to detect and target epicardial MLC2v phosphorylation levels in early disease).

Methods

Generation of gene-targeted mice. SM and DM mutant mice were generated by standard homologous recombination in an R1 ES cell line using targeting constructs that incorporated an SM of T to G in codon 15 or a DM from AG to GC in codon 14 and from T to G in codon 15 of *Mlc2v*, with the G418 resistance gene. Targeted ES cell clones were microinjected into C57BL/6 blastocysts to give rise to chimeric mice. Germline transmission of the disrupted allele was obtained and verified by DNA analyses, and mice were backcrossed to a C57BL/6 background for at least 10 generations. Refer to Supplemental Methods for details.

2D gel analysis. Multicellular myocardial preparations (600–900 mm × 100–250 mm) were isolated and homogenized from mouse hearts as previously described (29), with minor modifications. Myocardial homogenates were analyzed for nonphosphorylated and phosphorylated Mlc2v states using 2D gel electrophoresis in a mini gel system (Bio-Rad Laboratories) as previously described (28). Refer to Supplemental Methods for details.

Liquid chromatography–tandem mass spectrometry analysis. Myofilament proteins were isolated from mouse hearts as previously described (44). Protein samples were separated by 12% sodium dodecyl sulfate-polyacrylamide gel electrophoresis and visualized by Coomassie blue staining as previously described (44). The gel band corresponding to the Mlc2v protein (19 kDa) was excised and trypsinized as described by Shevchenko et al. (45). The extracted peptides were analyzed directly by liquid chromatography–tandem mass spectrometry (LC-MS/MS) using electrospray ionization. Refer to Supplemental Methods for details.

Phosphorylation assays. Mlc2v kinase reactions using cardiac and skeletal Mlck were done as described (28, 46). Refer to Supplemental Methods for details.

Ventricular weight to body weight ratios and histological analysis. Mice were anesthetized with ketamine/xylazine and weighed to determine total body weight. Hearts were removed, including all major vessels. Connective tissue and atria were also dissected away. The LV were separated, blotted, and weighed. Paraffin-embedded cardiac sections (8-μm thick) were stained with H&E and Masson's trichrome stain as previously described (47). A von Kossa (Sigma-Aldrich) staining assay was also performed on paraffin-embedded cardiac sections according to the manufacturer's instructions.

Echocardiography. Mice were anesthetized with 1% isoflurane and subjected to echocardiography as previously described (48).

Morphometric analyses of isolated adult mouse cardiac myocytes. Adult cardiac myocytes were isolated from mouse hearts as previously described (47). Cell length and width measurements were performed on isolated adult cardiac myocytes using NIH ImageJ software.

Electron microscopy. Electron microscopy was performed using standard procedures. Refer to Supplemental Methods for details.

RNA analysis. Total RNA was extracted from LV using TRIzol (Invitrogen). Dot blot analysis was performed as previously described (47).

Measurement of Ca^{2+}-mediated force dynamics in isolated intact papillary muscles. RV papillary muscles were isolated from mouse hearts and then mounted in a cardiac tissue culture chamber as previously described (47), with minor modifications. Ca^{2+} transients and twitch tension were measured simultaneously in isolated RV papillary muscles at 25°C and 37°C. Refer to Supplemental Methods for details.

Myofilament Ca^{2+} activation computational model with 3-state crossbridge cycle. A new computational analysis was created by incorporating representations of Mlc2v-p mechanisms into a Markov model of myofilament function (21), with minor modifications. Baseline and phosphorylation-dependent model parameters are given in Supplemental Tables 1 and 2, respectively. Refer to Supplemental Methods for details.

Muscle twitch dynamic simulations using new computational model. Muscle twitch simulations were performed using the new computational analysis. Parameters for twitch simulations are found in Supplemental Tables 1 and 2. Refer to Supplemental Methods for details.

Urea glycerol gel analysis method to quantify Mlc2v phosphorylation. Urea glycerol gels were prepared and run essentially as previously described (30, 49). Refer to Supplemental Methods for details.

Computational model of LV torsion. Computational predictions of LV torsion were done by incorporating LV geometry, deformation, myofiber orientation, afterload, conduction velocities, and Ca^{2+} transient and length-dependent contractile forces as well as Mlc2v phosphorylation-dependent myosin crossbridge kinetics into a finite element model of the mouse LV. Parameters used for the contraction model are given in Supplemental Tables 1, 2, and 4. Hemodynamic parameters and passive material properties are listed in Supplemental Tables 3 and 4, respectively. LV torsion and SWD were calculated in the LV finite element model as a function of MLC2v phosphorylation. Refer to Supplemental Methods for details.

MRI and LV torsion analysis. Refer to Supplemental Methods for details.

In vivo pressure overload model. Mice (6 weeks old) were anesthetized with ketamine/xylazine, and transverse aortic constriction (TAC) was performed as previously described (50). At 7 days following surgery, the pressure gradients generated by aortic banding were measured by introducing high-fidelity pressure transducers into the left and right common carotids.

Statistics. Data presented in the text and figures are expressed as mean values ± SEM. Significance was evaluated by the 2-tailed Student's *t* test or repeated measures ANOVA. For Kaplan-Meier survival analysis, significance was evaluated by the log-rank test. $P < 0.05$ was considered statistically significant.

Study approval. All animal procedures were approved by UCSD Animal Care and Use Committee.

Acknowledgments

We thank Jonathan Chang and Valeria Mezzano (UCSD) for technical assistance with histology and figures, respectively. We also thank the Farquhar Laboratory Transmission Electron Microscopy Core Facility (UCSD) for technical assistance with electron microscopy. We thank Mark Jutton (Scripps Research Institute, La Jolla, California, USA) for critical comments on the manuscript. This work was supported by grants from the NIH (to F. Sheikh, A.D. McCulloch, and J. Chen) and the National Biomedical Computation Resource (to A.D. McCulloch). F. Sheikh was a recipient of the National Scientist Development grant from the American Heart Association.

Received for publication September 23, 2011, and accepted in revised form January 18, 2012.

Address correspondence to: Farah Sheikh, Department of Medicine, University of California-San Diego, 9500 Gilman Drive, La Jolla, California 92093-0613C, USA. Phone: 858.246.0754; Fax: 858.822.1355; E-mail: fasheikh@ucsd.edu. Or to: Andrew McCulloch, Department of Bioengineering, University of California-San Diego, 9500 Gilman Drive, La Jolla, California 92093-0412, USA. Phone: 858.534.2547; Fax: 858.332.1706; E-mail: amcculloch@ucsd.edu. Or to: Ju Chen, Department of Medicine, University of California-San Diego, 9500 Gilman Drive, La Jolla, California 92093-0613C, USA. Phone: 858.822.4276; Fax: 858.534.2069; E-mail: juchen@ucsd.edu.

1. Spudich JA. The myosin swinging cross-bridge model. *Nat Rev Mol Cell Biol*. 2001;2(5):387–392.
2. Morita H, Seidman J, Seidman CE. Genetic causes of human heart failure. *J Clin Invest*. 2005; 115(3):518–526.
3. Ebashi S, Endo M. Calcium ion and muscle contraction. *Prog Biophys Mol Biol*. 1968;18:123–183.
4. Gordon AM, Homsher E, Regnier M. Regulation of contraction in striated muscle. *Physiol Rev*. 2000; 80(2):853–924.
5. Sweeney HL, Bowman BF, Stull JT. Myosin light chain phosphorylation in vertebrate striated muscle: regulation and function. *Am J Physiol*. 1993;264(5 pt 1):C1085–C1095.
6. Davis JS, et al. The overall pattern of cardiac contraction depends on a spatial gradient of myosin regulatory light chain phosphorylation. *Cell*. 2001; 107(5):631–641.
7. Hinken AC, Solaro RJ. A dominant role of cardiac molecular motors in the intrinsic regulation of ventricular ejection and relaxation. *Physiology (Bethesda)*. 2007;22:73–80.
8. Morano I. Effects of different expression and post-translational modifications of myosin light chains on contractility of skinned human cardiac fibers. *Basic Res Cardiol*. 1992;87 suppl 1:129–141.
9. Moss RL, Fitzsimons DP. Regulation of contraction in mammalian striated muscles—the plot thick-ens. *J Gen Physiol*. 2010;136(1):21–27.
10. Poetter K, et al. Mutations in either the essential or regulatory light chains of myosin are associated with a rare myopathy in human heart and skeletal muscle. *Nat Genet*. 1996;13(1):63–69.
11. Scruggs SB, et al. A novel, in-solution separation of endogenous cardiac sarcomeric proteins and identification of distinct charged variants of regulatory light chain. *Mol Cell Proteomics*. 2010;9(9):1804–1818.
12. Szczesna D, et al. Familial hypertrophic cardiomyopathy mutations in the regulatory light chains of myosin affect their structure, Ca^{2+} binding, and phosphorylation. *J Biol Chem*. 2001;276(10):7086–7092.
13. van Der Velden J, et al. Effects of calcium, inorganic phosphate, and pH on isometric force in single skinned cardiomyocytes from donor and failing human hearts. *Circulation*. 2001;104(10):1140–1146.
14. van Der Velden J, et al. Increased Ca2+ sensitivity of the contractile apparatus in end-stage human heart failure results from altered phosphorylation of contractile proteins. *Cardiovasc Res*. 2003;57(1):37–47.
15. Metzger JM, Greaser ML, Moss RL. Variations in cross-bridge attachment rate and tension with phosphorylation of myosin in mammalian skinned skeletal muscle fibers. Implications for twitch potentiation in intact muscle. *J Gen Physiol*. 1989; 93(5):855–883.
16. Colson BA, et al. Differential roles of regulatory light chain and myosin binding protein-C phosphorylations in the modulation of cardiac force development. *J Physiol*. 2010;588(pt 6):981–993.
17. Levine RJ, Kensler RW, Yang Z, Stull JT, Sweeney HL. Myosin light chain phosphorylation affects the structure of rabbit skeletal muscle thick filaments. *Biophys J*. 1996;71(2):898–907.
18. Greenberg MJ, Mealy TR, Watt JD, Jones M, Szczesna-Cordary D, Moore JR. The molecular effects of skeletal myosin regulatory light chain phosphorylation. *Am J Physiol Regul Integr Comp Physiol*. 2009;297(2):R265–R274.
19. Uyeda TQ, Abramson PD, Spudich JA. The neck region of the myosin motor domain acts as a lever arm to generate movement. *Proc Natl Acad Sci U S A*. 1996; 93(9):4459–4464.
20. Khromov AS, Somlyo AV, Somlyo AP. Thiophosphorylation of myosin light chain increases rigor stiffness of rabbit smooth muscle. *J Physiol*. 1998; 512(pt 2):345–350.
21. Campbell SG, Lionetti FV, Campbell KS, McCulloch AD. Coupling of adjacent tropomyosins enhance cross-bridge-mediated cooperative activation in a markov model of the cardiac thin filament. *Biophys J*. 2010;98(10):2254–2264.
22. Fitzsimons DP, Moss RL. Cooperativity in the regulation of force and kinetics of force development in heart and skeletal muscle: cross-bridge activation of force. *Adv Exp Med Biol*. 2007;592:177–189.
23. Swartz DR, Moss RL. Influence of a strong-binding myosin analog on calcium sensitive mechanical properties of skinned skeletal muscle fibers. *J Biol Chem*. 1992;267(28):20497–20506.
24. Dickinson MH, et al. Phosphorylation-dependent power output of transgenic flies: an integrated study. *Biophys J*. 1997;73(6):3122–3134.
25. Herring BP, Gallagher PJ, Stull JT. Substrate specificity of myosin light chain kinases. *J Biol Chem*. 1992; 267(36):25945–25950.
26. Sanbe A, et al. Abnormal cardiac structure and function in mice expressing non-phosphorylatable cardiac regulatory myosin light chain 2. *J Biol Chem*. 1999; 274(30):21085–21094.
27. Ikebe M, Hartshorne DJ, Elzinga M. Identification, phosphorylation, and dephosphorylation of a second site for myosin light chain kinase on the 20,000-dalton light chain of smooth muscle myosin. *J Biol Chem*. 1986;261(1):36–39.
28. Olsson M, Patel J, Fitzsimons D, Walker J, Moss RL. Basal myosin light chain phosphorylation is a determinant of Ca2+ sensitivity of force and activation dependence of the kinetics of myocardial force development. *Am J Physiol Heart Circ Physiol*. 2004; 287(6):H2712–H2718.
29. Stelzer JE, Patel JR, Moss RL. Acceleration of stretch activation in murine myocardium due to phosphorylation of myosin regulatory light chain. *J Gen Physiol*. 2006;128(3):261–272.
30. Hidalgo C, Wu Y, Peng J, Siems WF, Campbell KB, Granzier H. Effect of diastolic pressure on MLC2v phosphorylation in the rat left ventricle. *Arch Biochem Biophys*. 2006;456(2):216–223.
31. Stracher A. Evidence for the involvement of light chains in the biological functioning of myosin. *Biochem Biophys Res Commun*. 1969;35(4):519–525.
32. Weeds AG. Light chains of myosin. *Nature*. 1969; 223(5213):1362–1364.
33. Sweeney HL, Yang Z, Zhi G, Stull JT, Trybus KM. Charge replacement near the phosphorylatable serine of the myosin regulatory light chain mimics aspects of phosphorylation. *Proc Natl Acad Sci U S A*. 1994;91(4):1490–1494.
34. Henson RE, Song SK, Pastorek JS, Ackermann JJ, Lorenz CH. Left ventricular torsion is equal in mice and humans. *Am J Physiol Heart Circ Physiol*. 2000; 278(4):H1117–H1123.
35. Rüssel IK, Götte MJ, Bronzwaer JG, Knaapen P, Paulus WJ, van Rossum AC. Left ventricular torsion: An expanding role in the analysis of myocardial dysfunction. *JACC Cardiovasc Imaging*. 2009; 2(5):648–655.
36. Sester RM, Kasper JM, Lieber ML, Starling RC, McCarthy PM, White RD. Persistent abnormal left ventricular systolic torsion in dilated cardiomyopathy after partial left ventriculectomy. *J Thorac Cardiovasc Surg*. 2003;126(1):48–55.
37. Fuchs E, Müller MF, Oswald H, Thöny H, Mohacsi P, Hess OM. Cardiac rotation and relaxation in patients with chronic heart failure. *Eur J Heart Fail*. 2004; 6(6):715–722.
38. Gotte MJ, et al. Myocardial strain and torsion quantified by cardiovascular magnetic resonance tagging: studies in normal and impaired left ventricular function. *J Am Coll Cardiol*. 2006; 48(10):2002–2011.
39. Laser KT, et al. Is torsion a suitable echocardiographic parameter to detect acute changes in left ventricular afterload in children? *J Am Soc Echocardiogr*. 2009;22(10):1121–1128.
40. Tan YT, et al. The pathophysiology of heart failure with normal ejection fraction: exercise echocardiography reveals complex abnormalities of both systolic and diastolic function involving torsion, untwist, and longitudinal motion. *J Am Coll Cardiol*. 2009;54(1):36–46.
41. Vannan MA, et al. Effect of cardiac resynchronization therapy on longitudinal and circumferential left ventricular mechanics by velocity vector imaging: description and initial clinical application of a novel method using high-frame rate B-mode echocardiographic images. *Echocardiography*. 2005;22(10):826–830.
42. Brecker SJD. The importance of long axis ventricular function. *Heart*. 2000;84(6):577.
43. Gautel M. Cytoskeletal protein kinases: titin and its relations in mechanosensing. *Pflugers Arch*. 2011; 462(1):119–134.
44. Tong CW, Gaffin RD, Zawieja DC, Muthuchamy M. Roles of phosphorylation of myosin binding protein-C and troponin I in mouse cardiac muscle twitch dynamics. *J Physiol*. 2004;558(pt 3):927–941.
45. Shevchenko A, Wilm M, Vorm O, Mann M. Mass spectrometric sequencing of proteins silver-stained polyacrylamide gels. *Anal Chem*. 1996;68(5):850–858.
46. Chan JY, et al. Identification of cardiac-specific myosin light chain kinase. *Circ Res*. 2008; 102(5):571–580.
47. Sheikh F, et al. An FHL1-containing complex within the cardiomyocyte sarcomere mediates hypertrophic biomechanical stress responses in mice. *J Clin Invest*. 2008;118(12):3870–3880.
48. Cheng H, et al. Loss of enigma homolog protein results in dilated cardiomyopathy. *Circ Res*. 2010; 107(3):348–356.
49. Granzier HL, et al. Truncation of titin's elastic PEVK region leads to cardiomyopathy with diastolic dysfunction. *Circ Res*. 2009;105(6):557–564.
50. Rockman HA, et al. Segregation of atrial-specific and inducible expression of an atrial natriuretic factor transgene in an in vivo murine model of cardiac hypertrophy. *Proc Natl Acad Sci U S A*. 1991; 88(18):8277–8281.